Measuring Charged Particle Beam Fluence Beyond 10^{15} n_{eq}/cm^2 Using Planar and 3D Silicon Diodes

By

Ivan V. Rajen

Advisors: Sally Seidel and Martin Hoeferkamp

Honors Thesis
University of New Mexico
Dept. of Physics and Astronomy
May 2018

Abstract

The Pixel detector in the ATLAS Experiment at the Large Hadron Collider at CERN is exposed to extremely high radiation over the lifetime of its use. Upgrades to the Pixel detector for the High Luminosity Large Hadron Collider (HL-LHC) require components that have demonstrated performance at the relevant radiation levels. New technologies proposed for the upgrades are irradiated by our UNM group at the 800 MeV proton LANSCE facility in Los Alamos National Laboratory to verify their operation and radiation hardness up to HL-LHC fluences. I investigated the use of planar and 3D diodes to measure the profile and fluence of the charged particle beam in real time. I developed the hardware and software required to use 3D diodes to measure fluence, and I optimized the operation of planar diodes for fluence measurements. Both the planar and 3D devices are shown to meet requirements for effective real-time fluence and beam profile measurements.

1.0 Introduction

A program has been undertaken to develop the best possible method for real-time measurements of charged particle fluence and beam profile. Applications of two types of semiconductor diode, operated in different modes and with different characteristics, are compared. The method involves construction of a device, described below, that incorporates the diodes. In one version, the device uses pin silicon diodes, which have the property that their measured voltage in forward bias grows linearly with fluence under certain conditions. In the other version, employing diodes of the 3D design, leakage current is linearly proportional to fluence when they are operated in reverse bias mode. Arrays of the sensors are constructed on printed circuit boards. When an array is placed in the path of a charged particle beam, the profile of the beam can be mapped by measuring the forward voltage or leakage current respectively, of the diodes. New detectors for use in the High-Luminosity Large Hadron Collider (HL-LHC) inner detector must be verified to operate up to $2x10^{16}$ 1-MeV n_{eq}/cm^2. To test their radiation hardness, they are irradiated with charged beams. Those beams must be characterized. This requirement motivates this project.

1.1 Radiation Damage of Detectors at the Large Hadron Collider

The Large Hadron Collider is located at CERN (European Organization for Nuclear Research) in Switzerland and is the largest, most advanced, and highest energy particle accelerator in the world. Several experiments are conducted at the LHC, including: ATLAS (A Toroidal LHC ApparatuS), CMS (Compact Muon Solenoid), LHCb (LHC-

beauty), and ALICE (A Large Ion Collider Experiment). The LHC will be upgraded to the HL-LHC (High Luminosity Large Hadron Collider) by the year 2025 which will increase its luminosity by a factor of ten. Increasing the luminosity will increase the rate of particle interactions in the detectors and these interactions cause damage leading to degradation and eventual failure in all materials present. The increase in interactions will call for electronic devices and sensors that are ten times as radiation hard as the present ones.

1.2 Pixel Detector and Irradiation Campaigns

Our UNM group collaborates with the ATLAS experiment on the upgrade of the Pixel detector. The Pixel detector is the innermost detector in the ATLAS experiment and is responsible for tracking charged particles. As the innermost detector it is exposed to the highest amount of radiation. Estimates show that the Pixel detector will be exposed to up to 2×10^{16} n_{eq}/cm^2 over 10 years in HL-LHC conditions. The symbol "n_{eq}" stands for "1-MeV-neutron-equivalent." It normalizes the damage caused by particles of a variety of energies and species to a single standard. Our group has led irradiations at the Los Alamos Neutron Science Center (LANSCE) for over ten years to test detectors proposed for the LHC upgrade. At LANSCE we use an 800 MeV proton beam to irradiate devices. Aluminum foil dosimeters have been used to measure radiation fluences, however that method, which uses radioactive decay measurements, can only be applied offline after the experiment has been concluded. The silicon diode-based system described here is effective because it allows for real-time electronic readout.

2.0 Semiconductors

The devices that were developed for this project use semiconductor technology. Semiconductors are materials that exhibit both conducting and insulating properties. The most common semiconductor is silicon. The electrons bound to the silicon atoms in a crystal lattice have allowed quantum wave functions based on the periodic potential created by the ions that comprise the lattice. Due to the close spacing of allowed energy levels for the wave functions of the many atoms ($\sim 10^{22}$/cm^3 in a lattice) and the Pauli Exclusion Principal restricting electrons from sharing the same state, electrons in the bulk material occupy distinct energy bands called the valence and conducting bands. When the energy gap between bands is large, the valence electrons in the material are difficult to excite into the conduction band; such materials are insulators. When the bands overlap, the electrons are free to move between the bands; such materials are usually metals and are conductors. If the gap between bands is narrow, at low temperatures the material will be an insulator, and at higher temperatures the material will be a conductor; this is a semiconductor. Figure 2.1 illustrates these cases.
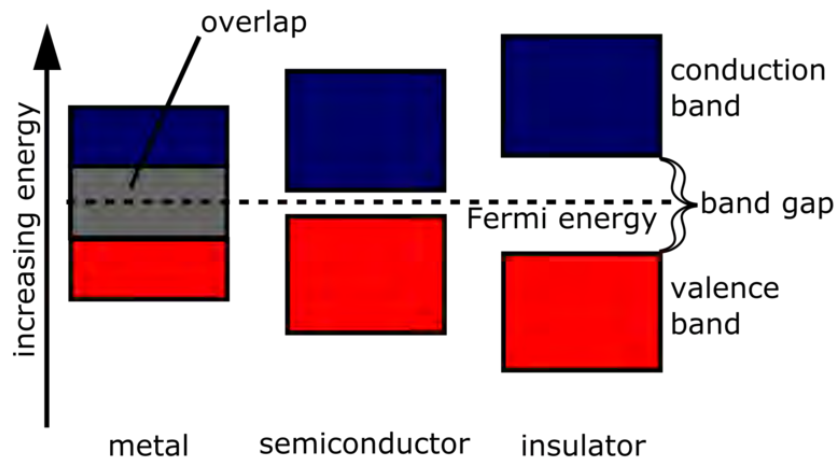

Fig. 2.1: Band structure of a metal, semiconductor, and insulator. [1]

2.1 PN Junctions

When an electron crosses the band gap, a hole is left in the place of the empty bond. Semiconductor materials may be doped with atoms that have more or fewer valence electrons than the intrinsic semiconductor material. Boron, aluminum, and gallium have fewer valence electrons than silicon and are called p-type (positive) dopants. Phosphorous, arsenic, and antimony have more valence electrons than silicon and are called n-type (negative) dopants. Figure 2.2 shows what doped silicon looks like visually using the atomic orbital model.
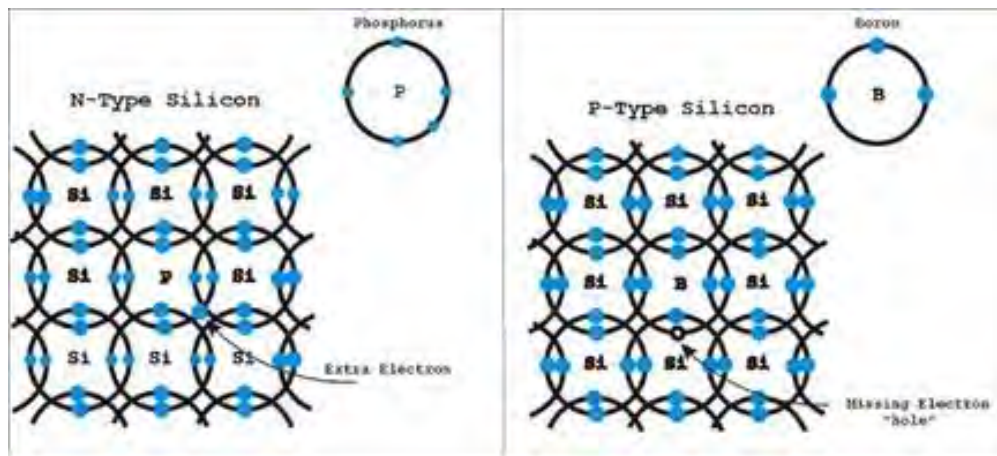

Fig. 2.2: N-doped silicon (left) and p-doped silicon (right). [2]

Doping will result in an excess of holes or electrons and will increase the conductivity of the semiconductor. When two semiconductors of types p and n are brought into contact, they can form a pn junction. At the interface of the p and n regions electrons and holes diffuse and create a charge-neutral region with a built-in electric field; this is called the depletion region. Figure 2.3 shows the interface of a pn junction, and the behavior under forward and reverse bias.
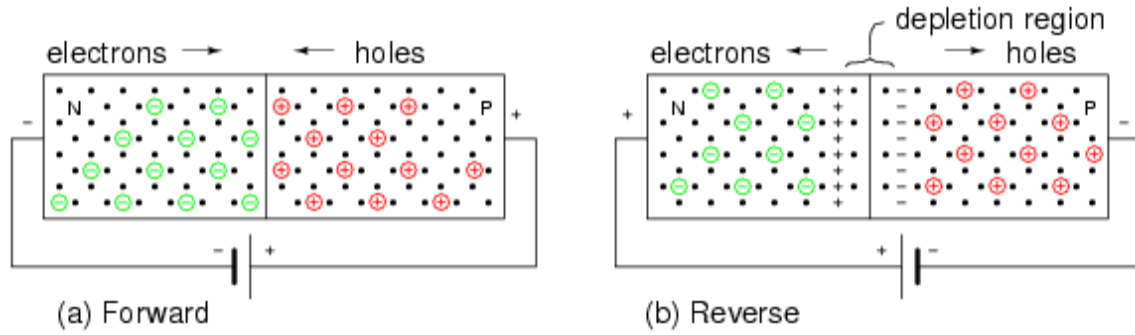
Fig. 2.3: A pn junction in forward bias (a) and reverse bias (b) [3].

When voltage is applied across the pn junction in forward bias, the free electrons and holes at the n and p boundary will drift in the applied field. If the applied voltage is greater than the built-in electric field, the diode will pass current through; this voltage is called the threshold voltage. Voltage applied in the reverse direction will expand the depletion region towards the physical limit of the diode. When the depletion region extends through the entire volume of the semiconductor, the diode is fully depleted; the voltage at which this occurs is the depletion voltage. This behavior is shown in plots of current vs. voltage (IV curves). The ideal IV characteristics of diodes are shown in figure 2.4.
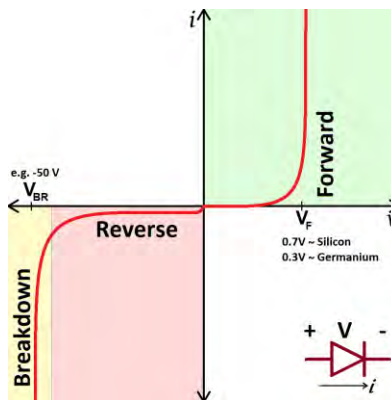

Fig. 2.4: Current-voltage characteristic of a pn diode. Leakage current is shown in the pink shaded region and is the reverse biased current before breakdown. V_F is the threshold voltage and V_{BR} is the breakdown voltage. [4]

In reverse bias the diode will sustain current due to minority carriers in the p and n regions; this is called leakage current. If enough reverse bias is applied, the diode will break down. Zener breakdown and avalanche breakdown are the two phenomena by which this can occur. Zener breakdown is more typical for highly doped pn junctions, and is the result of electrons tunneling from the n to the p side. Avalanche breakdown occurs when the minority electrons are given a high enough kinetic energy to free electrons in the p side of the semiconductor. The result is that electrons multiply and there will be an exponential increase in current. The voltage at which breakdown occurs is called the breakdown voltage. The pn junction is the basis of the solid-state semiconductor diode. Diodes that have large breakdown voltage, low leakage current, and depletion voltages much less than breakdown are desired for operation in reverse bias mode.

2.2 Sensors

Application of reverse bias to a diode that is fully depleted places the diode in a state where the volume is charge neutral and sustains an electric field. A charged particle incident on the diode will transfer some of its energy to ionization in the lattice, producing a track of electron-hole pairs. The electrons and holes will drift along the lines of the electric field. Structures designated as p+ and n+ use highly doped materials. The '+' indicates doping concentrations of three orders of magnitude greater than normal doping concentrations. These electrons and holes can then be collected by highly doped p+ and n+ structures respectively acting as electrodes and read out as a signal. The time of arrival at each electrode allows for the reconstruction of the particle's path. The electrons are read out in the devices I studied, as they drift faster than holes in the semiconductor, due to the electrons having higher mobility.

2.3 Planar Diodes

A planar sensor can be constructed with a base substrate of n doped material. The bottom surface is implanted or sputtered with n+ doped material while the top surface has strips or pixels of p+ doped material. The p+ electrode is used to collect the electron current to reconstruct the particle path. Figure 2.5 shows the behavior of a planar sensor when a charged particle leaves a track of electron-hole pairs.
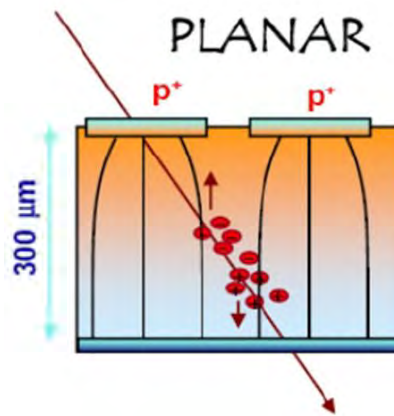

Fig. 2.5: Planar diode used as a sensor. [5]

2.4 3D Sensors

3D sensors were first described in 1996 [6]. They are different from planar sensors in that the p+ and n+ electrodes are oriented perpendicularly to the wafer surface, as cylindrical columns through the n type substrate, rather than on the top and bottom surfaces. The distance between electrodes in a planar sensor is the thickness of the sensor, while the distance between electrodes in a 3D sensor is the spacing between the p+ and n+ columns. The smaller width between p+ and n+ electrodes decreases the voltage needed to deplete the diode in reverse bias, which increases the operating range of the sensor. The smaller width also increases the electric field between electrodes, which allows signals to be read out faster and decreases the chance of signal electrons being caught in

charge traps produced by defects in the silicon lattice after heavy irradiation. Figure 2.6 shows the behavior of a 3D sensor when a charged particle leaves a track of electron-hole pairs; the smaller distance between p+ and n+ terminals shows that electrons travel a shorter distance and are in a stronger electric potential.
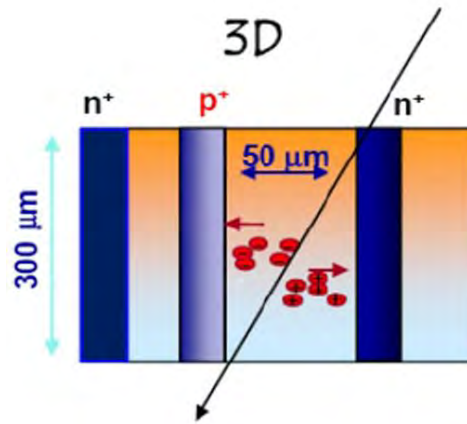

Fig. 2.6: 3D diode used as a sensor. [7]

2.5 Radiation Measurement

There is a relationship between the charged particle fluence silicon diodes receive, and their characteristics in forward bias and reverse bias. In forward bias, diodes have greater resistance after irradiation, and in reverse bias, diodes sustain higher leakage current after irradiation [8]. High-energy charged particle radiation can cause displacement damage within the semiconductor lattice of the diode. Since displacement damage is directly related to the number of particles incident on a semiconductor lattice, there is a correlation between radiation received and changes in diode characteristics. In forward bias there is a linear increase in forward voltage V_F, due to a linear decrease in free charge carrier concentration [8]:

$$V_F \propto \phi_{eq}$$

9

Where ϕ_{eq} is the fluence normalized to 1-MeV neutrons (the relationship is calibrated with aluminum foil dosimeters). In reverse bias there is a linear increase in minority charge carriers [8], leading to the relation

$$\Delta I = \alpha \phi_{eq} V$$

where ΔI is the change in leakage current, ϕ_{eq} is the fluence normalized to 1-MeV neutrons, V is the depleted volume of the diode, and α is the current related damage coefficient. The factor α varies with post-irradiation time and temperature due to annealing of the diode [8]. The linear correspondence allows for a mapping of measured forward voltage or measured leakage current to fluence. Diodes placed in an array can then image a charged particle beam, as each diode in the array can be read out to indicate the amount of fluence it received.

2.6 Radiation Hardness

A radiation imaging and measurement system is needed because the next-generation particle tracking sensors proposed for use at the LHC need to be verified to operate past fluences of 10^{16} n_{eq}/cm^2. The semiconductor diodes used for particle tracking have been designed to be radiation hard. Radiation hardness is achieved by design to optimize diode characteristics and operation. A sensor needs to reliably track charged particles over the lifetime of its use. Since the sensors are operated in reverse bias at the depletion voltage, the prevalent task is to design a diode that has low depletion voltage, low leakage current, high breakdown voltage, and fast readout of signals.

3.0 Building the Array of 3D Diodes

Eighty-eight 3D diodes manufactured by FBK in Trento, Italy were acquired. The diodes were produced with eight layouts determined by their dimensions and whether or not they

utilize a guard ring. The purpose of a guard ring is to shield the active area of the sensor from diffusion current by shaping the electric field. The dimensions of the 3D sensors are a measure of the horizontal and vertical dimensions of the pixel cells on each chip (Fig. 3.1). Pixel cell dimensions affect the radiation hardness and characteristics of the sensor. The operating range of a 3D diode is between the depletion voltage and the breakdown voltage. The radiation hardness requirement in particle tracking is sufficient depletion at voltages lower than breakdown. Irradiating diodes will increase the depletion and breakdown voltages of the diodes. Thus, it was necessary to characterize all diodes to verify their performance and to find a roughly homogeneous group of diodes from which to produce a diode array.

3.1 Cataloguing

To start, I inspected every 3D sensor under a microscope. Each sensor is marked to indicate manufacturer, dimension, and GR, 2E, or 3E. The label GR means guard ring, while 2E and 3E are a count of the n+ columns in a pixel cell (2E indicating two and 3E indicating three n+ columns).
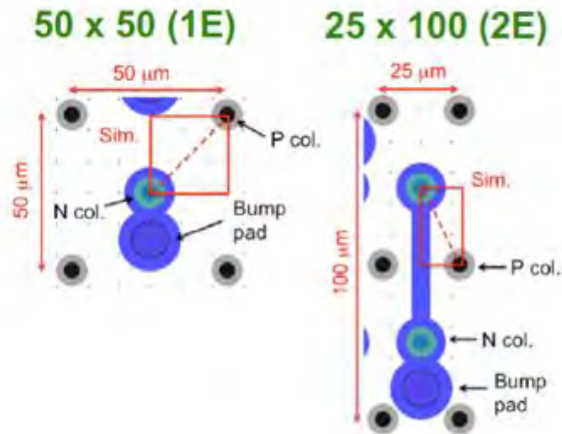
Fig. 3.1: Layout of the 3D diodes examined. On the left is a 1E diode with a spacing of 50μm between columnar electrodes of the same doping type, corresponding to ~35μm between columns of opposite type. On the righthand side is a 2E diode with spacing of 25μm between columnar p+ electrodes and 50μm between columnar n+ electrodes, corresponding to ~28μm between columns of opposite type. [9]

The eight types of diodes are shown in table 3.1.

Diode Name	Type	Dimensions
3D diode CMS	GR	50x100
3D diode CMS	3E	50x100
Diode	3E	50x125
Diode	GR	50x125
R Diode	3E	50x90
R Diode	GR	50x90
3D DiodeCMS	GR	25x100
3D DiodeCMS	2E	25x100

Table 3.1: Catalog of the 88 diodes; there were on average 11 diodes per type.

The nominal thickness of the active area is 130 microns. The thickness and the area of the

diode are used to calculate the depletion volume, which is a factor in relating leakage

current to fluence. Using the microscope I made measurements of the dimensions of the

sensors to verify the values in the order sheet. I mount each sensor to the microscope

stage, I then measure the sensor thickness by first focusing the microscope on its stage. I

then raise the microscope and stop when the sensor top surface is in focus. The amount I

raised the microscope to change the focus from the stage to the sensor surface is the

thickness. Initially I observed unexpected values for thicknesses, which were reconciled

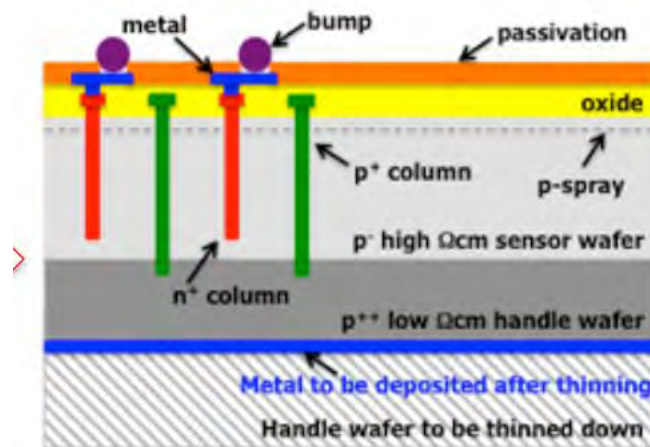by the fact that the sensors are fabricated on a support wafer (Fig. 3.2).

Fig. 3.2: Schematic cross section of the 3D sensors under study:

with passing-through junction p+ electrodes; with partially-through junction n+

electrodes. The main sensor wafer is attached to a support wafer, labeled "Handle

wafer" here. [10]

The support wafer provides stability and physical resilience to the fragile and thin

sensors. I also encountered an unforeseen issue when investigating the backside of the

sensors. The sensors came attached to dicing tape. The dicing tape left a residue on some

of the sensors (Fig. 3.3) and inadvertently added a small thickness as well as some electrical insulation.
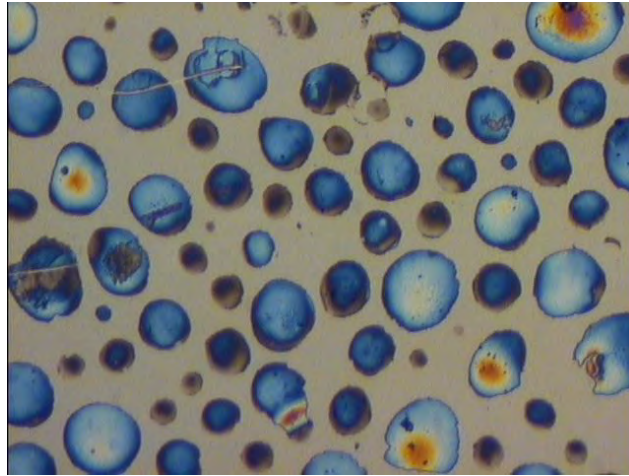

Fig. 3.3: Dicing tape residue on the back side of a 3D sensor.

The sensors without the residue were of roughly the same thickness: 250 microns. The sensor thickness measured will not be used in calculation of the depletion volume; the support wafer adds undepleted material that must not be counted toward the actual thickness of the depleted volume. The manufacturer of the 3D diodes measured the thickness of the active volume to be ~130 microns.

3.2 Characterization

Diode characterization is the second step. Characterization involves determining the electrical properties of each diode. Since the 3D diodes will be used in reverse bias, only properties pertaining to this mode were examined. The leakage current, breakdown voltage, and depletion voltage were the three characteristics I investigated. I measured the current-versus-voltage (IV) characteristic of each 3D diode, and used them to find the leakage current and the breakdown voltage. There are two methods to find the depletion voltage: the first method is to measure the capacitance-versus-voltage (CV) characteristic

of each 3D diode, and the second method is to shine a laser on the 3D diode and measure the response as a function of bias voltage.

3.3 Leakage Current and Breakdown Voltage

The probe station is used to facilitate electrical measurements of semiconductor devices. Probes in micro-positioners are used for stable and precise operation of devices without the need for permanent wire connections. Tungsten electrodes are used to apply bias voltage via the contact pads on the 3D sensors. The tungsten electrodes have extremely sharp tips that are placed on the contact pads using precise probe manipulators. The microscope that is part of the probe station is used for careful placement of the tungsten tip. The chuck of the probe station has a small hole for suction of the backside of the diode. The vacuum allows for good electrical contact of the base of the diode, or its negative terminal. I used a LabView program to apply a range of bias voltages and acquire current data; from these I made IV plots. The IV plots are necessary to reveal any 3D diodes with defects that produce high leakage currents or low breakdown voltages. Figure 3.4 shows some of the IV curves for the diodes that could be characterized with the probe station. 3D diodes that broke down at low bias voltage or had relatively high leakage currents were ruled out of consideration for the diode array. Leakage current level is indicated in fig 3.4 where the current is relatively constant, and breakdown voltage is where the current increases exponentially. The preferential diodes have leakage currents of ~100 picoamperes ($1x10^{-10}$ A) and breakdown voltages of over 100 Volts.
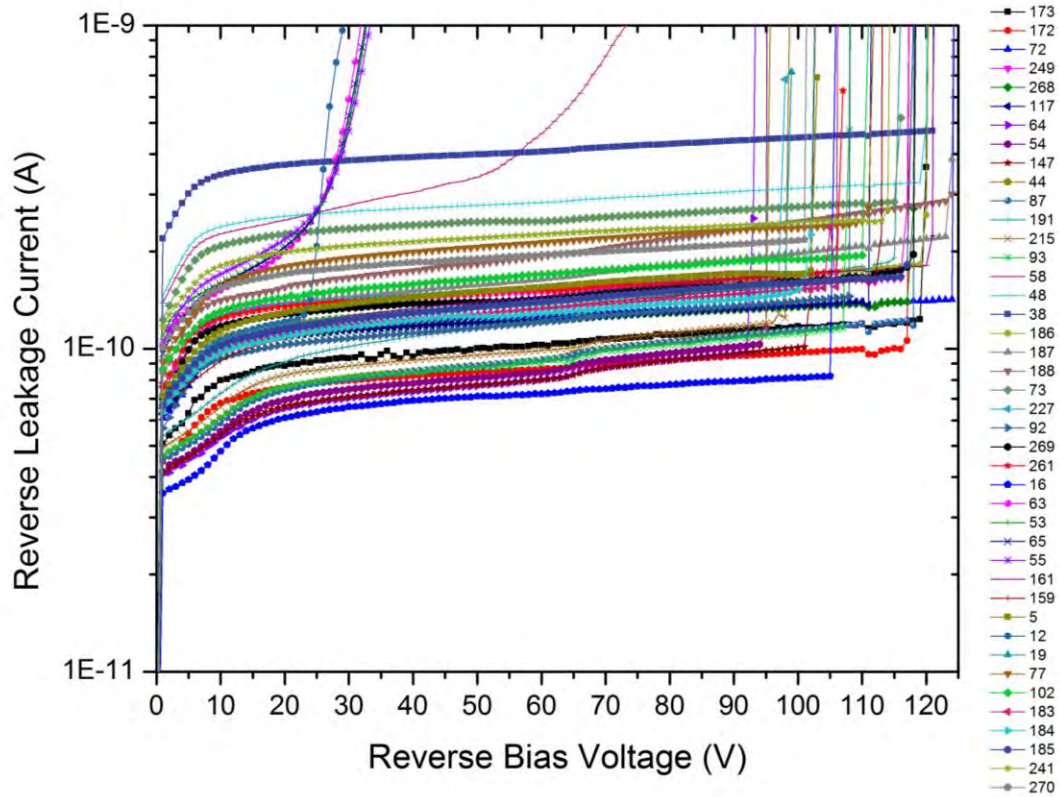
Fig. 3.4: Reverse leakage current versus reverse bias voltage characteristics for 42 diodes from the 88 diodes. The legend indicates the diode identification number.

3.4 Depletion Voltage

Capacitance versus bias voltage measurements and laser measurements are done using the probe station and a LabView application. To determine the depletion voltage from a CV curve I fit two lines along the distinct regions of the curves: a line fit on the region of positive slope, and a line fit to the plateau. The intersection of these two lines is defined as the depletion voltage (Fig. 3.5).
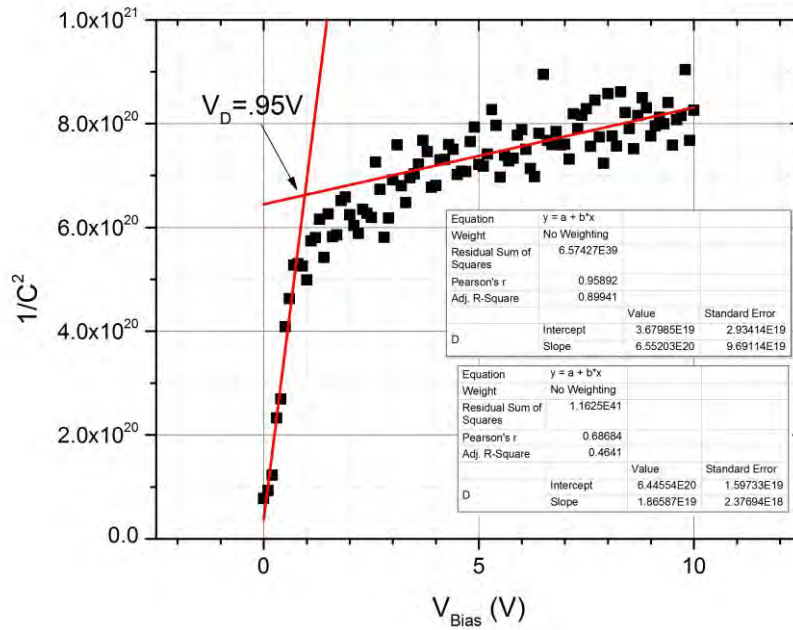
16

Equation	y = a + b*x	
Weight	No Weighting	
Residual Sum of Squares	6.57427E39	
Pearson's r	0.95892	
Adj. R-Square	0.89941	
	Value	Standard Error
D Intercept	3.67985E19	2.93414E19
D Slope	6.55203E20	9.69114E19

Equation	y = a + b*x	
Weight	No Weighting	
Residual Sum of Squares	1.1625E41	
Pearson's r	0.68684	
Adj. R-Square	0.4641	
	Value	Standard Error
D Intercept	6.44554E20	1.59733E19
D Slope	1.86587E19	2.37694E18

Fig. 3.5: Determination of depletion voltage using the capacitance-voltage relationship.
Laser measurements make use of the sensor properties of the diodes. A diode used as a sensor will output a signal when a charged particle or photon creates electron-hole pairs along its track in a depleted volume. I shined an infrared laser of 1060 nm wavelength (sufficient to penetrate the active thickness of the silicon) on the sensor while applying varying levels of bias voltage to the diode. Using an oscilloscope I measured the signal produced by the sensor. The signal in millivolts vs. bias voltage is plotted. I fit lines to the region of positive slope and the plateau and locate their intersection, which defines depletion (Fig. 3.6). To accommodate the microstructure of the device, depletion voltage can also be defined as the point where the signal is 90% of the maximum signal. The CV method is automated and faster to perform, however since the 3D diode manufacturing process is new and unoptimized some diodes presented nonstandard CV curves. The only way to determine the depletion voltage for some diodes was to use the laser method.
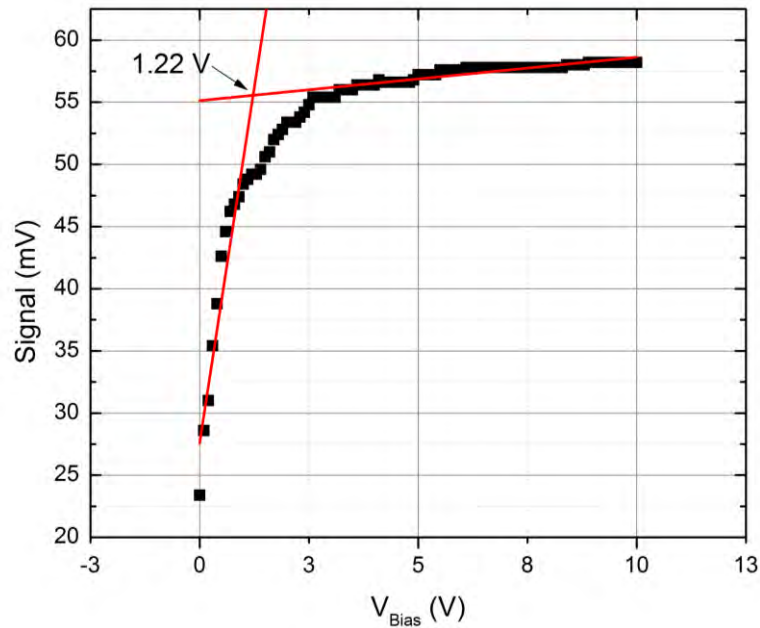
Fig. 3.6: Determination of depletion voltage using a laser: signal amplitude is graphed versus applied bias voltage.

3.5 Diode Selection

Of the 88 diodes characterized, I found a group of 28 usable 3D diodes. The printed circuit boards that the diodes are mounted on can support 7 rows by 7 columns of diodes. For this reason, it is necessary to find multiples of 7 usable diodes to be able to symmetrically profile a beam. The diodes I chose had similar leakage currents and similar breakdown voltages. In some cases I was unable to characterize a diode with the probe station, as some displayed open circuit behavior or low breakdown voltage and high leakage current.

3.6 Wire Bonding

A typical 3D pixel has dimensions 2 mm x 2 mm, and their contact pads have areas typically of a few hundred square micrometers. The small size requires the use of wire

bonds to make connections from the diode to the board. I bonded the 28 diodes to the board (fig. 3.7).
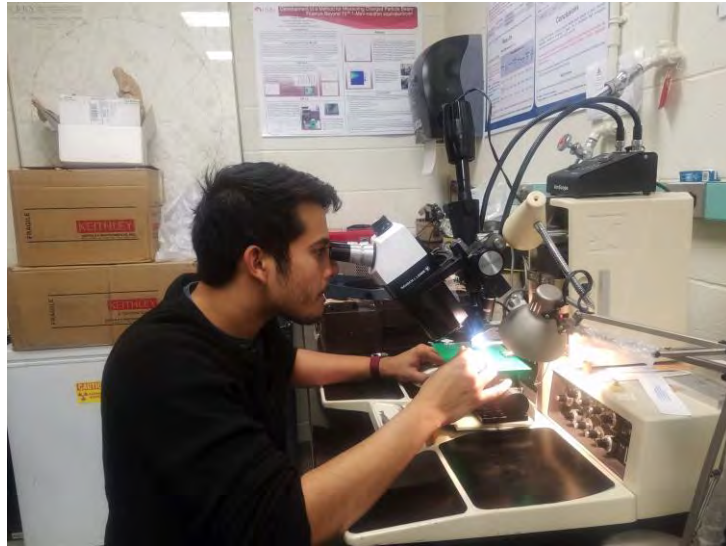

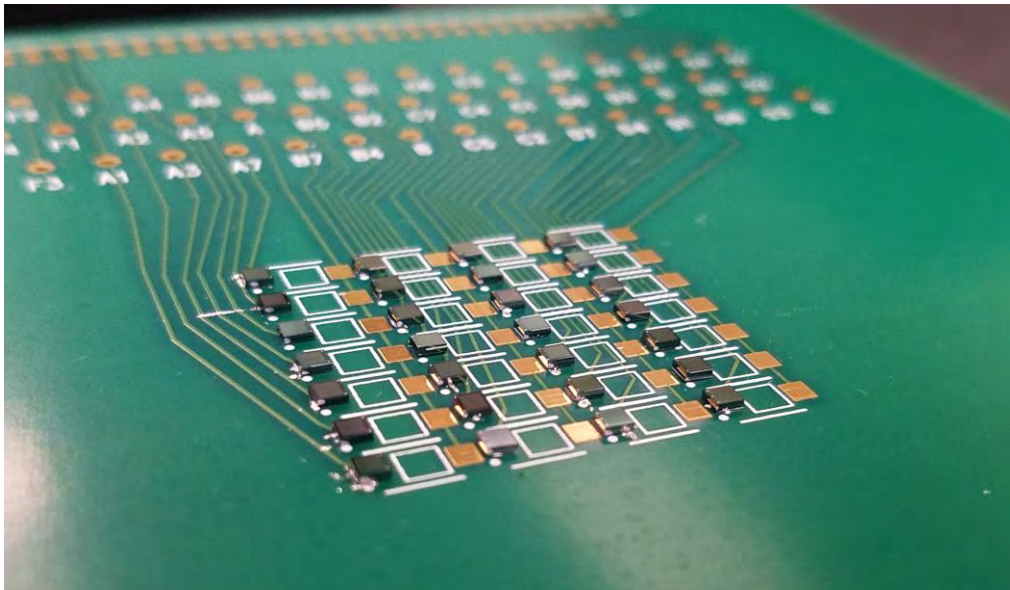*Fig. 3.7: Wire-bonding machine and process.*

Fig. 3.8: Fully assembled 3D diode board.

3.7 Hardware Selection

Dynamic range and signal level are necessary considerations in determining what hardware should be used for the test stand to read out the diode arrays. The leakage

current of the diodes prior to irradiation ranged from 30 pA to 300 pA. The diode leakage current will increase linearly over the range of 10^{12} to 10^{16} n_{eq}/cm^2, which means the ammeter needs dynamic range from picoamperes to microamperes. In addition I used a scanner to switch between diodes, and the scanner needs to support low current switchboards. The Keithley 3706 scanner, Keithley 3761 10-channel Low Current Multiplexer cards, and Keithley 6487 picoammeter fit the current range requirement. To run a set of measurements on the diode board, a ribbon cable is connected from the diode board to a converter box that maps each channel from the ribbon cable to a coaxial cable in an array. The coaxial outputs of the array are connected to the Keithley 3761 Low Current Multiplexer cards in the 3706 scanner. The 6487 picoammeter is connected to the 3706 to apply voltage and measure the current of each diode. LabView controls each Keithley device.
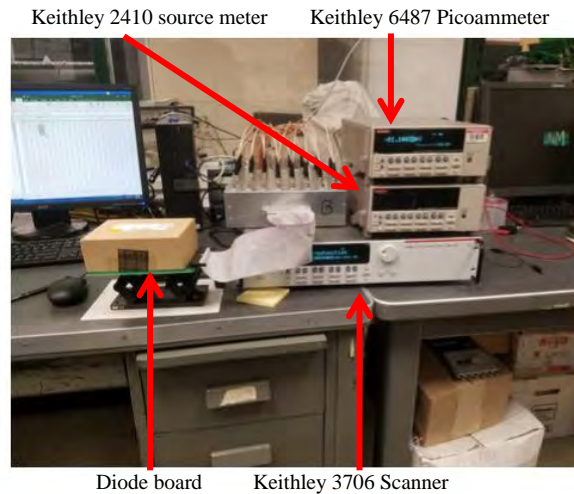

Fig. 3.9: Test stand and the devices used.

3.8 LabView Code

I developed LabView code for leakage current measurements of 3D diodes to complement existing LabView code for forward voltage measurements of planar diodes.

The LabView algorithm is as follows: close the channel of the diode being measured, apply a voltage greater than the depletion voltage and lower than the breakdown voltage, measure the leakage current, open the channel, and repeat the process for subsequent diodes. Organization of the data involved the following challenges. Each diode is mapped to a coordinate in X and Y on the diode board. The diode board I built is designed in a 7x4 layout, however future boards might have different dimensions and other characteristics. I added inputs for the number of columns and rows, number of diodes, and spatial separation between columns and rows so that the output is a 3-column data file with leakage current, X position, and Y position in a format that a ROOT program can automatically assemble into a 3D surface plot. A screenshot image of the LabView program is shown in figure 3.9.
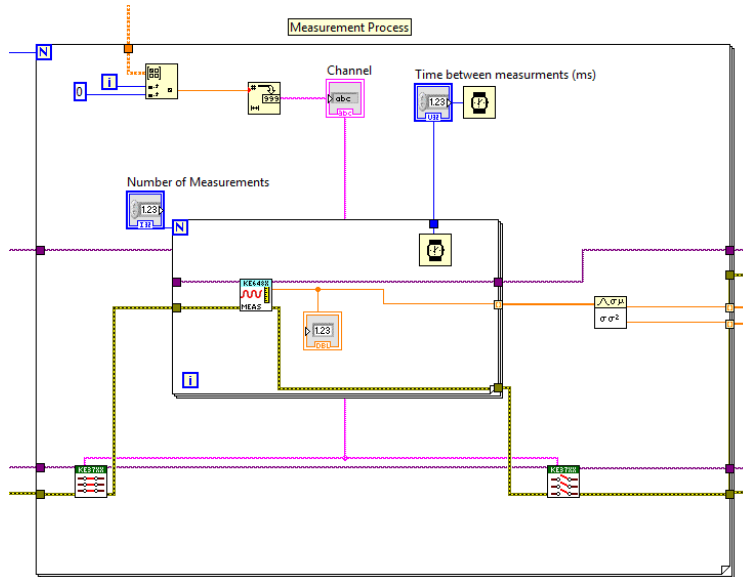

Fig. 3.10: Screen-capture of LabView block diagram made to automate 3D sensor measurements. A loop takes current measurements for each diode. The rest of the LabView code organizes the data to be surface plotted on an XY plane matching the layout of the board.

3.9 Test

The test stand and LabView code were verified with an irradiated 3D diode board. The irradiated board is a 3x4 array of 12 diodes with a pitch between columns and rows that is different from the pitch of the board I built. This helped to test the flexibility of the LabView application. I connected the 3D diode board to the test stand and entered the dimensions for the board. This produced a data file from which I made a plot of the fluence as a function of diode position on the board (Fig. 3.10). 3D plots in ROOT utilize a stitching algorithm that makes surface plots visually easy to comprehend.
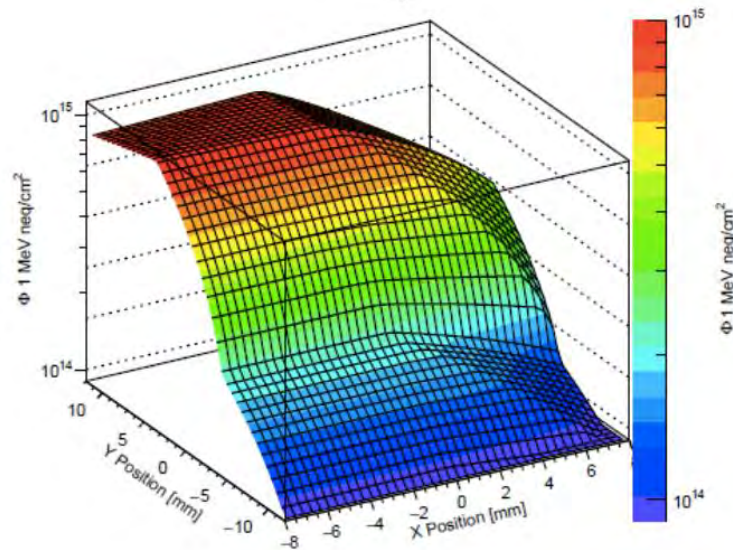

Fig. 3.11: Beam profile of previously irradiated 3D diode board using data automatically collected by LabView. The data are plotted in ROOT, which interpolates between points to provide a more structured surface.

4.0 Optimizing the Operation of the Array of Planar Diodes

An irradiated planar diode board was previously assembled but not optimized. Planar diodes had been previously shown [11] to be linear in voltage versus fluence in the range of $2x10^{12}$ to $2x10^{14}$ n_{eq}/cm^2 fluences.
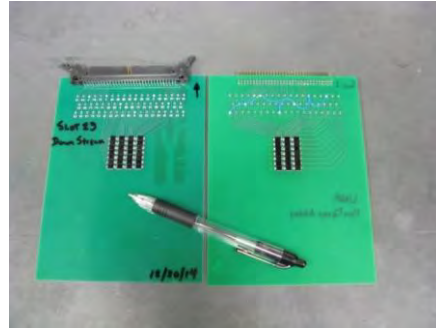
Fig. 4.1: Two UNM planar diode boards, showing the front and back of a diode board.

I investigated the measurement system to see if changing how the current is applied could extend the linear regime. I examined signals from the test stand with an oscilloscope (Fig. 4.2).
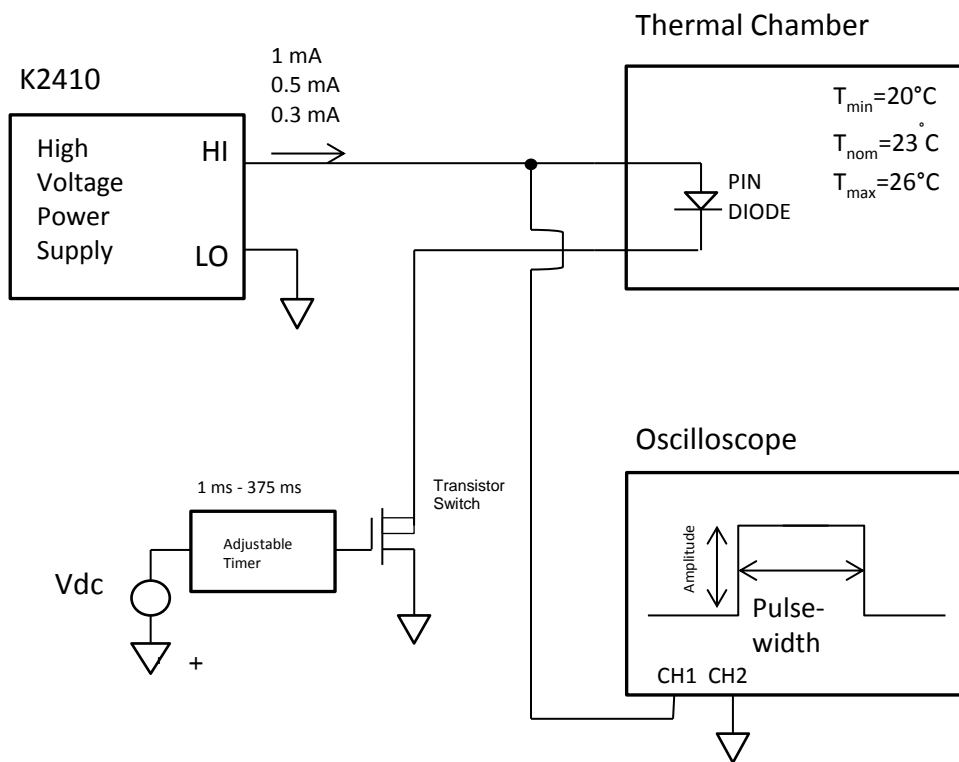

Fig. 4.2: Test stand used to examine the planar diode measurement system.

4.1 Pulse Width

I observed that the voltage decreased over the duration of application of the current pulse. Joule heating is thought to cause nonlinear diode response. Diode voltage decreases with increased temperature, so the longer current pulses are applied, the more they heat the diode and decrease the forward voltage over the course of the measurement [12]. Since the voltage decreases throughout the measurement process, the average value is lower than it would be if it had not sustained heating. I studied the effect of pulse width by examining the voltage response to pulse widths of 372 ms, 50 ms, and 5 ms. Figure 4.3 shows currents applied for 372 ms (upper left); 50 ms (upper right); and 5 ms (lower). One sees that the voltage decays steeply over the course of the 372 ms pulse, however for 5 ms pulses the voltage is relatively constant and is what we define now as the optimal pulse width.
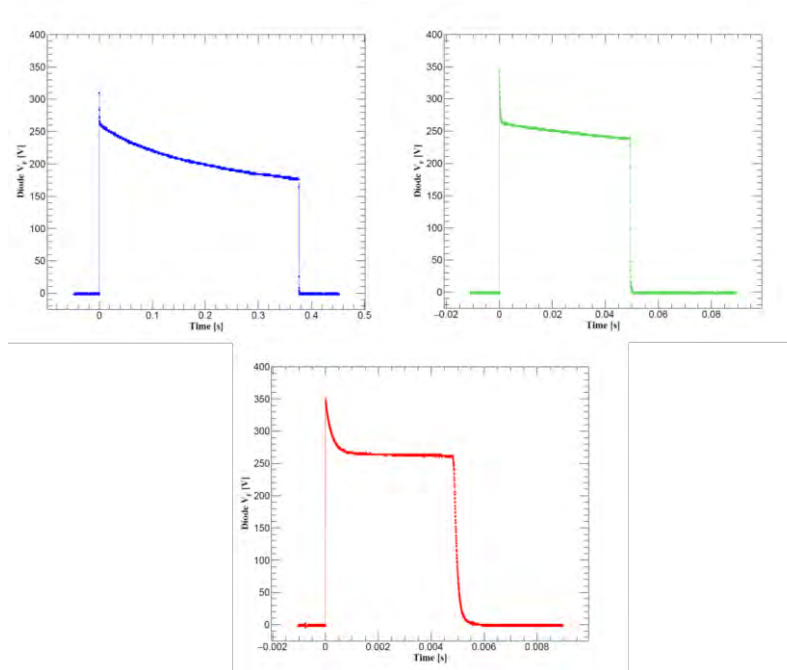

Figure 4.3: Voltage response over the interval of applied current pulse. Top left 372 ms, top right 50 ms, bottom 5 ms. [13]

4.2 Current Level

The current amplitude applied to the diodes affects the measured forward voltage. I investigated the effect of various current amplitudes to extend the linear region of fluence vs. voltage. I applied 0.3 mA, 0.5 mA, and 1 mA current levels and discovered that the lower currents became nonlinear at a fluence of 5×10^{14} n_{eq}/cm^2. The 1 mA current retains the linear characteristic beyond that point. I selected 1 mA and 5 ms pulse width to provide linearity over the largest fluence range. Figure 4.4 shows the measured diode voltage versus fluence for three levels of applied current. The outcome is: I extended the fluence range of the planar diodes to 3.79×10^{15} n_{eq}/cm^2 by optimization of the current level and pulse width. This represents a roughly 20 times increase over the previously reported rage of linearity.
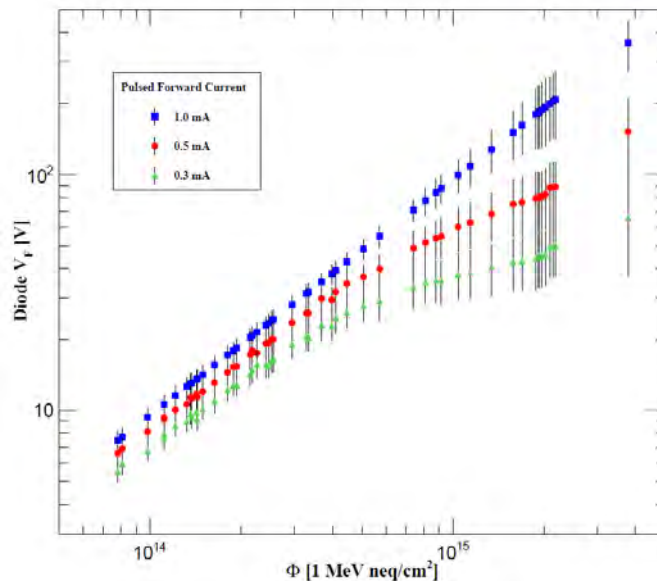

Fig. 4.4: Fluence versus voltage at three current levels for 5 ms pulses. [13]

4.3 Temperature Effects

I determined the error associated with taking measurements in an environment that may vary in ambient temperature. The irradiation facility is roughly room temperature, and additionally the proton beam may transiently heat the diodes and other materials, so the temperature can vary over a range of a few degrees. I took forward voltage measurements at 20°C, 23°C, and 26°C to establish the systematic error due to temperature. I found that the uncertainty is less than 10% for fluences below 5×10^{14} n_{eq}/cm^2, the uncertainty increases to 16% at 10^{15} n_{eq}/cm^2, and it reaches 30% above 2×10^{15} n_{eq}/cm^2 (Fig. 4.5).
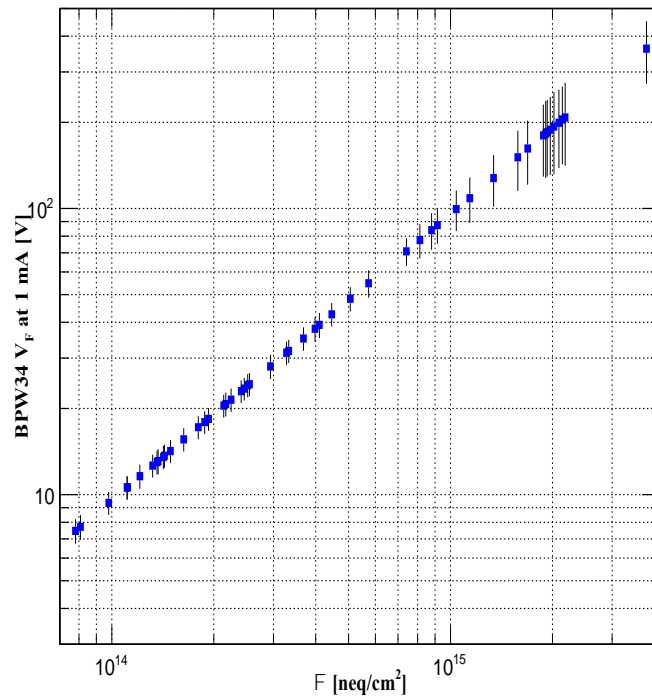

Fig 4.5: Uncertainty on voltage due to temperature variation of ±3 degrees Celsius relative to 23°C.

5.0 Conclusions

Planar and 3D diodes are viable technologies for the purpose of real-time fluence measurements. Planar diodes were demonstrated to provide a linear relationship between fluence and voltage up to approximately 4×10^{15} n_{eq}/cm^2. A potential limitation is the magnitude of the voltages measured as fluence increases. The diode exposed to the highest fluence read out voltages of over 300 volts. An exposure of 2×10^{16} n_{eq}/cm^2 could be monitored by successive installation of 5 or 6 planar diode arrays, as each board could measure $\sim 4 \times 10^{15}$ n_{eq}/cm^2 for a combined total of $\sim 2 \times 10^{16}$ n_{eq}/cm^2. 3D diodes maintain low leakage currents even at high fluences, which is an attractive feature. A full 3D diode array has been built for this thesis and will be tested in an active proton beam, at LANSCE in late 2018.

Acknowledgments

References

[1] Wikipedia Commons, Band Gap Comparison,

https://commons.wikimedia.org/wiki/File:Band_gap_comparison.svg

[2] Images Scientific Instruments, Semi-Conductors used in Photovoltaic Cells,

https://www.imagesco.com/articles/photovoltaic/photovoltaic-pg2.html

[3] All about circuits, The PN junction,

https://www.allaboutcircuits.com/textbook/semiconductors/chpt-2/the-p-n-junction/

[4] Spark of fun, Diodes, https://learn.sparkfun.com/tutorials/diodes

[5] Helmuth Spieler, Semiconductor Detector Systems, Oxford University Press 2005.

[6] S.I. Parker et al., "3-D: A New Architecture for Solid State Radiation Detectors,"
Nucl. Instr. and Meth. A 395 (1997) 328-343.

[7] S.I. Parker and C. Kenney, "Performance of 3-D Architecture Silicon Sensors After
Intense Proton Irradiation," IEEE Transactions on Nuclear Science, Vol. 48, No. 5,
October 2001.

[8] M. Moll, "Radiation Damage in Silicon Particle Detectors," Ph.D. thesis, Univ.
Hamburg, 1999.

[9] D.M.S. Sultan et al., JINST 12 (2017) C01022.

[10] C. Kenney, et al., "Silicon Detectors with 3-D Electrode Arrays: Fabrication and
Initial Test Results," IEEE Transactions on Nuclear Science, Vol. 46, No. 4, August
1999.

[11] P. Palni, et al., "A method for real time monitoring of charged particle beam profile
and fluence," Nuclear Instr. and Meth. A 735 (2014) 213-217.

[12] F. Ravotti, "Development and Characterization of Radiation Monitoring Sensors for the High Energy Physics Experiments of the CERN LHC Accelerator," Dissertation, Université Montpellier II, 2006 (unpublished).

[13] M.R. Hoeferkamp, et al., "Application of p-i-n photodiodes to charged particle fluence measurements beyond 10^{15} 1-MeV-neutron-equivalent/cm^2," Nuclear Instr. and Meth. A 890 (2018) 108-111.